

## Effect of Brass Solder Composition on Quality in Laser Soldering of Solar Panel Busbar

Wei Xiaohua<sup>1</sup>, Zheng Mingliang (0000-0001-5681-0051)<sup>2\*</sup>

<sup>1</sup>School of Mechanical and Electrical Engineering, Quzhou College of Technology, Quzhou 324000, China.

<sup>2</sup>School of Mechanical and Electrical Engineering, Huainan Normal University, Huainan 232038, China. E-mail: [liangmingzheng@hnnu.edu.cn](mailto:liangmingzheng@hnnu.edu.cn)

In order to reveal the action mechanism of different brass solder compositions on the microstructure of weld joints in unleaded-tin-coated coppers brazing-stitch soldering, the laser soldering process of solar panel busbar was studied by using three different coated brass solders: Sn-37Bi-3Ag, Sn-42Bi-3Ag and Sn-47Bi-3Ag. Scanning electron microscope, energy spectrometer, X-ray diffractometer, tensile testing machine and Vickers microhardness tester were used to test and analyze the influence of Bi element content on the microstructure and mechanical properties of weld joints in solar panel busbar brazing-stitch soldering. The results show that: (1) With the increase of Bi element content, the wettability of soldering seam is gradually improved, and the weld joints eutectic mainly consists of SnAg phase, Ag<sub>3</sub>Sn phase, Cu<sub>6</sub>Sn<sub>5</sub> phase, Cu<sub>3</sub>Sn phase, SnAgCu phase,  $\beta$ -Sn solid solution and Bi with rhombic layered structure. (2) The fracture of weld joints occurred at the interconnection belt side, it presents brittle and ductile mixed fracture. With the decrease of Bi element content, the tensile strength of weld joints gradually increased, and the maximum tensile strength of weld joints was 212 MPa. (3) The tensile strength of weld joints decreases gradually from the busbar side to the interconnection belt side, and the highest microhardness of weld joints appears at the interface layer, it can reach 330.1 HV. With the decrease of Bi element content, the microhardness of weld joints gradually increased. This paper provides a scientific basis for the optimal selection and use of busbars in solar panels high-quality laser soldering.

**Keywords:** Solar Panel Busbar, Laser soldering, Sn-Bi-Ag Brass Solder, Microstructure, Mechanical Properties

### 1 Introduction

Busbar soldering is a crucial link in the production of solar panel modules, and its soldering performance directly determines the working efficiency of the panel [1]. The solar panel busbar soldering is to connect the interconnection belts on two adjacent battery strings together by means of stitch soldering, which plays the role of parallel battery strings. Among them, the busbar and the interconnection belt are both tin-coated copper alloys, so it belongs to the stitch soldering of the same alloy [2]. During soldering, the soldering heat source heats the soldering strip to a temperature higher than the melting point of the tin solder but lower than the melting point of the base metal oxygen free copper. After the tin solder melts, it has a certain fluidity and can wet the base metal. After the tin solder is cooled and solidified, the interconnection belt and the busbar are connected. However, due to the difficulties such as the shape warping of busbar and interconnecting belt, and the high temperature sensitivity (optimal temperature is 240°C- 280°C) [3], so it is of great engineering value to develop high-quality soldering methods suitable for solar panel busbar.

At present, the commonly used soldering technologies of solar panel busbar include electric soldering

iron, electromagnetic soldering and infrared lamp heating soldering. But the electric soldering iron is low life and low stability [4], the electromagnetic soldering technology has the problem that the flux will crystallize on the surface of the battery panel and the energy will be wasted seriously [5], the main disadvantage of infrared lamp heating soldering technology is that the heating area is large, which affects the packaging of solar panel modules [6]. Compared with traditional soldering methods, laser soldering is an important application field of laser additive manufacturing. Laser soldering has the characteristics of high power density, small heat input and heat affected area, and is easy to realize automation, fast soldering speed, and accurate and adjustable heat input [7-14]. Therefore, in terms of the heat source quality and the degree of automation, laser soldering is the best soldering method for interconnection belts and busbars. Now, many scholars have carried out a lot of research on laser soldering of copper alloy materials. Anil Kunwar [15] studied the effect of heat and mass transfer of laser soldering on the growth behavior of intermetallic compounds in Sn/Cu and Sn-3.5, Ag-0.5/Cu joints, and predicted the interface morphology of intermetallic compound Sn-xAg-yCu/Cu (SAC/Cu) using a

data-driven method combined with laser soldering experiments, finite element analysis and machine learning. Nabila [16] studied the influence of optical fiber laser parameters on the interface reaction and wetting angle of two different types of solder pastes SAC305 on copper pads. Martin [17] studied the resistance of soldered battery cells. Zhou [18] used different Zn-Al components to explore the influence of Al content change in soldering wire on the microstructure and mechanical properties of Al/Cu welded joints. However, there is little research on the application of laser soldering technology in solar panel busbar. Some valuable literature on laser welding, such as Pavel [19], Ikhsan [20], Ondrej [21], these studies indicate that laser welding technology is an advanced material manufacturing technique

In this paper, the laser brazing and stitch soldering of the unleaded tin-coated coppers was carried out, focusing on the comparative analysis of the influence of the coated brass solder with different Bi element contents on the welded joint morphology, microstructure and mechanical properties. The research purpose of this paper is to reveal the mechanism of Bi element of

brass solder in the process of laser melt brazing to regulate the weld microstructure and performance, and lay a theoretical foundation for the application of laser melt brazing in the field of solar panel soldering.

## 2 Experimental materials and method

The base metal of busbar is TU1 oxygen free copper sheet, its length, width and thickness are 600mm×100mm×0.35mm. The base metal of interconnection belt is also TU1 oxygen free copper sheet, its length, width and thickness are 200mm×40mm×0.15 mm, These base metals are both in rolled and annealed state. The brass solder is tin solder. The Table 1 is the specific composition of different brass solder alloys used in this experiment. The base metals are coated brass solder by hot dip galvanizing, and the thickness of brass solder coating is 0.025 mm. The interconnection belt and busbar are assembled by vertically butted from the top to bottom, and the two sides are aligned without slope. The clamping device is used to clamp them on the phenolic insulation board.

**Tab. 1** Alloy Composition of brass solder

Order number	Brass solder	Alloy Composition (wt.%)		
		Sn	Bi	Ag
1	Sn-37Bi-3Ag	60	37	3
2	Sn-42Bi-3Ag	55	42	3
3	Sn-47Bi-3Ag	50	47	3

The laser spot is aligned with the long center line of base metal contact surface, and a medium power continuous fiber laser (GCL-500) is selected. Its technical parameters are shown in Table 2. The specific

parameters of laser are determined as the power  $P=400\text{W}$  and the soldering speed  $v=10\text{mm/s}$  by consulting the datum.

**Tab. 2** Technical parameters of continuous fiber laser

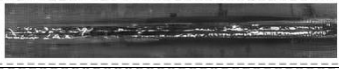

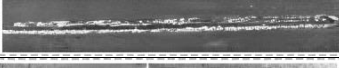
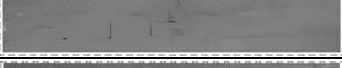
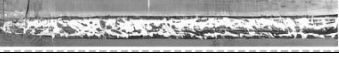

Model	Polarization	Rated power	Wavelength	Spectral width
Continuous	Random	530W	1080nm	3nm
Red light power	BPP	NA	Switching phototime	Modulation frequency
0.1mW	SMF 0.4	0.12	20ns	20kHz

Before soldering, the test piece shall be strictly cleaned, and the oxide film on the surface shall be removed with flux. After soldering, cutting out a 10mm×10 mm metallographic sample along the cross section of weld line, and put it into the inlaid prototype to make sample for easy grinding and polishing, then use a cotton swab to dip a small amount of aqua regia corrosion the sample for about 5 seconds. Finally, we use a scanning electron microscope (SEM, EVO18), a energy dispersive spectrometer (EDS,

Link-ISIS) and a X-ray diffraction (XRD-6000) to analyze the influence of different brass solder compositions on the surface morphology of the welded joints. For mechanical properties of welded joints, cutting out some tensile samples according to GB/T2651-2008 standard, and we use electronic universal testing machine to conduct tensile test under room temperature and tensile rate is 3mm/min. Recording the maximum load on the sample during the tensile test, repeating the test five times and taking the average value

of the maximum loads, the average value of the maximum loads is the tensile strength of the welded joint. For the fracture, we use SEM to observe the fracture morphology and analyze the fracture type of the welded joint. For the hardness, we use a full-automatic Vicker microhardness meter (Dure Scan) to test the hardness of the welded joint.

**Tab. 3** Macroscopic morphology of the front and back under different brass solder

Order number	Brass solder	Macroscopic morphology	
		Front	Back
1	Sn-37Bi-3Ag		
2	Sn-42Bi-3Ag		
3	Sn-47Bi-3Ag		

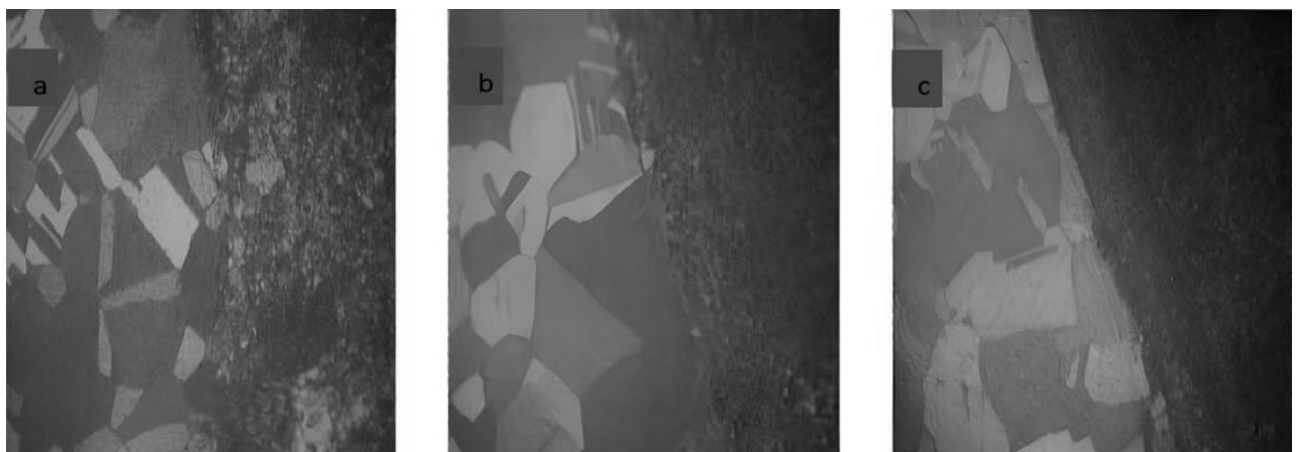
It can be seen from Table 3 that for brass solders with different Bi element contents, the surface of welded joints have different shapes, have not the soldering defects, and have the obvious metallic luster. When the Bi element content is 37% in brass solder, black oxide is generated on the front side of the welded joint. When the Bi element content is 42% and 47%, the wettability and spreadability on the front side are both good, the front side of the welded joints are both uniform and continuous, and the back sides only show light yellow due to thermal effect, which indicates the penetration is deeper, and the width of welded joint in the third group experiment is the largest. Therefore, the macroscopic morphology of busbar laser welded joint can be improved by adjusting the composition of coated brass solder.

The Figure 1 is the microstructure morphology of the welded joint near the base metal area of interconnection belt under coated brass solders with different

### 3 Microstructure of welded joints

The macroscopic morphology of the front and back sides of welded joint formed by using four different coated brass solder compositions are shown in Table 3.

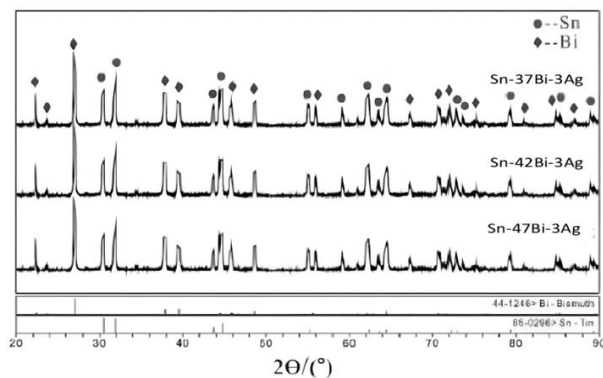
Bi element content. The left side of Figure is the weld area, which is mainly composed of spherical rich equiaxed crystals and black carbides, the right side is the base metal area, and the middle is the interface area. The Figure 1(a) is Sn-37Bi-3Ag coated brass solder, the Figure 1(b) is Sn-42Bi-3Ag coated brass solder, the Figure 1(c) is Sn-47Bi-3Ag coated brass solder. With the increase of Bi element content, the content of dissolved base metal Cu decreases, the compound reaction in the welded joint decreases, the thickness of the formed interface layer also decreases, and the interface layer gradually becomes flat and smooth, and the structure of the transition layer gradually disappears. The thickness of fusion line in interface area is Figure 1(a) 2.70 $\mu\text{m}$ , Figure 1(b) 2.32 $\mu\text{m}$  and Figure 1(c) 1.98 $\mu\text{m}$ . It can be seen that the thickness of the interface area decreases with the increase of Bi element content in coated brass solder.



**Fig. 1** Microstructure of the weld joints with different Bi content

The Figure 2 is the XRD phase analysis atlas of welded joints in the coated brass solders with different Bi element contents. It can be seen from Figure 2 that the grayish phase with low contrast is Sn, the white phase with high contrast is Bi, and the formed phase

between Ag and Sn is ephase, namely dark Ag<sub>3</sub>Sn. With the increase of Bi element content, the brittle blocky area (Bi) increases and segregation becomes more obvious.

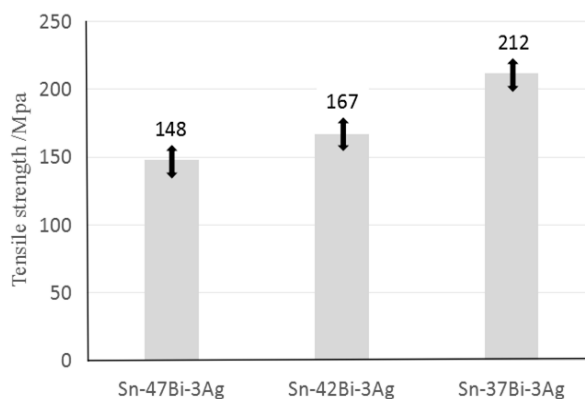


**Fig. 2** XRD analysis of the weld joints with different Bi content

#### 4 Mechanical properties of welded joints

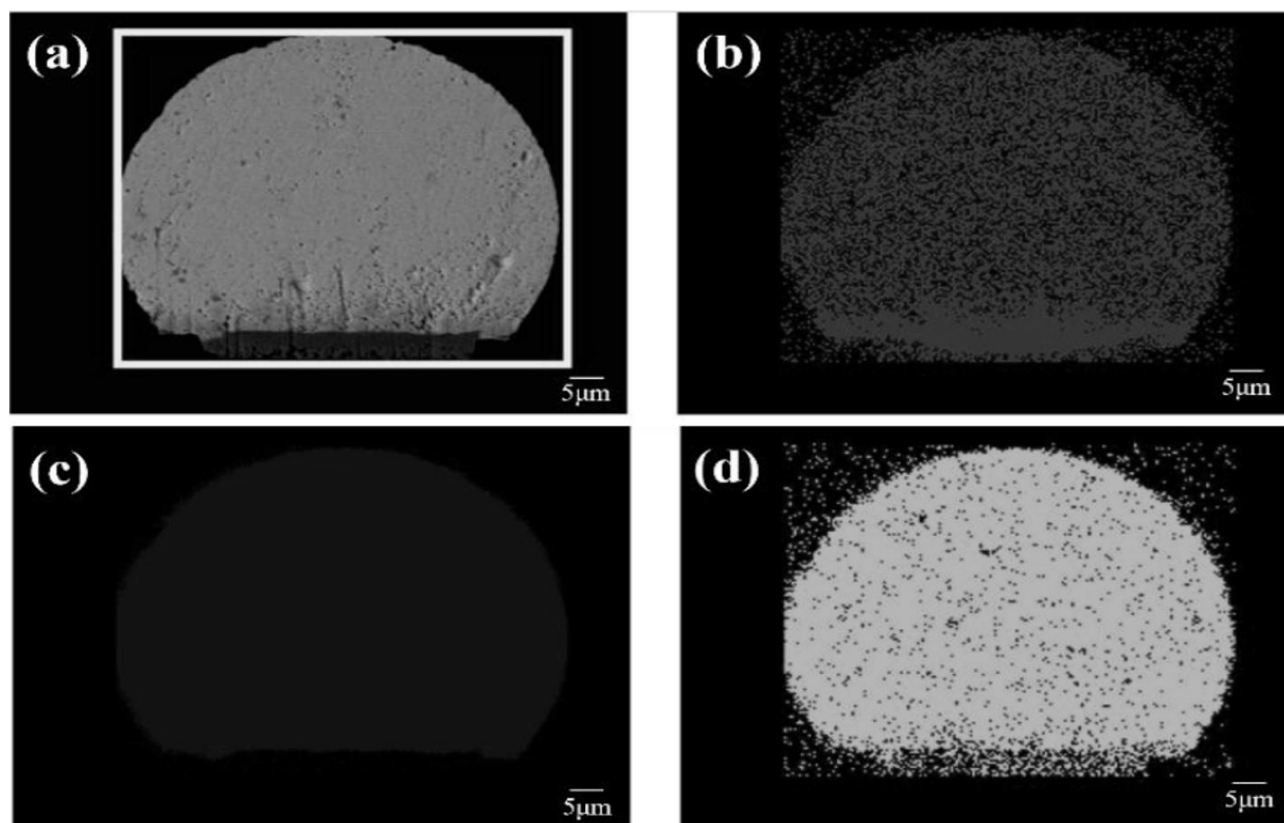
The Figure 3 is the influence of the coated brass solder with different Bi element contents on tensile strength of welded joints. The fracture of tensile specimen occurred at the welded side of interconnection belt. It can be seen from Figure 3 that with the decrease of Bi element content in the brass solder, the tensile strength of the joint is gradually increasing. When the coated brass solder is Sn-47Bi-3Ag, the tensile strength of the joint is 137MPa. With the decrease of Bi element content, when the coated brass solder is Sn-42Bi-3Ag, the tensile strength of the joint is 179MPa. When the coated brass solder is Sn-37Bi-3Ag, the tensile strength of the joint will further increase to 204MPa. This is because with the increase of Bi

element content in the coated brass solder, the brittle area (Bi phase) is increasing, and the segregation is more obvious. Although the solid solution and precipitation of Bi in the Sn matrix will increase the strength of the solder alloy, resulting in a small number of intermediate phases, namely, Ag<sub>3</sub>Sn phase, therefore, the ability to block the movement of particle dislocations is weakened, resulting in poor strengthening effect and reduced plasticity and toughness, so the tensile strength will decrease with the increase of Bi element content.



**Fig. 3** Tensile strength of tensile samples

In order to investigate the composition of intermetallic compounds at the interface, EDX was used to perform surface element scanning on laser brazed micro solder joints.

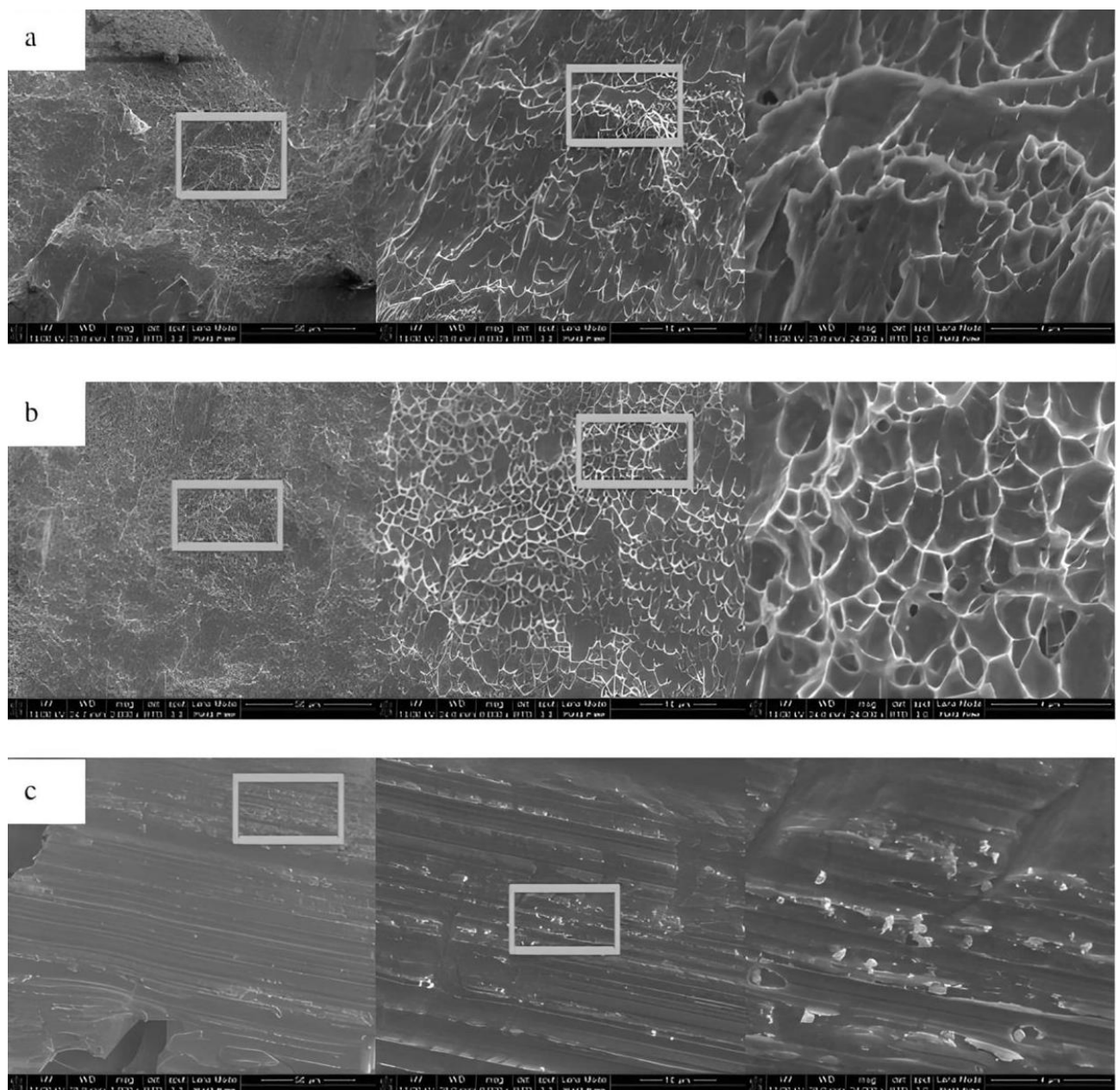


**Fig. 4** EDX element distribution of Sn42Bi3Ag initial micro-joints

From the EDX scan of the initial micro solder joint in Figure 4, (a) is SEM image, (b) is Ag element, (c) is Sn element, (d) Bi element. It can be seen that Ag atoms in the solder react with spontaneously diffusing Bi atoms at the solder pad and Sn inside the solder to form Ag-Bi-Sn ternary compounds. Most of the Ag phase and Sn phase are evenly distributed in the brazing material structure, while some Ag phase aggregates. A large number of Bi atoms were found above the solder pad, and the distribution of Ag layer did not completely cover the entire interface, indicating that Bi atoms were involved in the interface reaction process.

The Figure 5 is the fracture location and SEM micrograph of the fracture surface for the tensile specimen welded joint in coated brass solder with different Bi element contents. The fracture occurs at the

the interconnection belt welded side. It can be seen from Figure 5, when the coated brass solder is Sn-37Bi-3Ag, Figure 5 (a) shows that the fracture surface has dimples and tear edges of different sizes, which are characterized by ductile fracture; When the coated brass solder is Sn-42Bi-3Ag, Figure 5 (b) shows that the fracture surface has densely distributed dimples on the fracture surface, and some dimples are relatively larger and deeper. After secondary magnification, small dimples can also be seen near the larger dimples, which is shown as ductile fracture; When the coated brass solder is Sn-47Bi-3Ag, Figure 5 (c) shows that the fracture surface is relatively flat, showing brittle fracture, which is easy to crack when subjected to external tension. This result is consistent with the tensile strength result in Figure 3 and Figure 4.



**Fig. 5** Microscopic morphology of tensile fracture

It extends upward along the center of the molten pool at the busbar end to the top of the interconnection belt, the Figure 6 is the microhardness distribution of the welded joint under coated brass solder with different Bi element contents. It can be seen from Figure 6 that the hardness value increases gradually from the interconnection belt side to the busbar side, and the hardness value of the molten pool closer to the busbar side is larger. This is because the weldpool is subject to the dual effects of the Marangoni effect and metal vapor pressure, resulting in a "vortex" phenomenon, which involves the some liquid at the bottom end of interconnection belt toward the center of the weldpool, thus increasing the microhardness of the weldpool center. However, when there are defects such as pores in the welded joint, the microhardness will change suddenly. Significantly, with the decrease of Bi element content, the grains at the weldpool are refined continuously, and the precipitates of metal compounds are increased continuously, so the hardness of the welded joint is increased continuously. This result is consistent with the tensile strength result in Figure 3 and Figure 4.

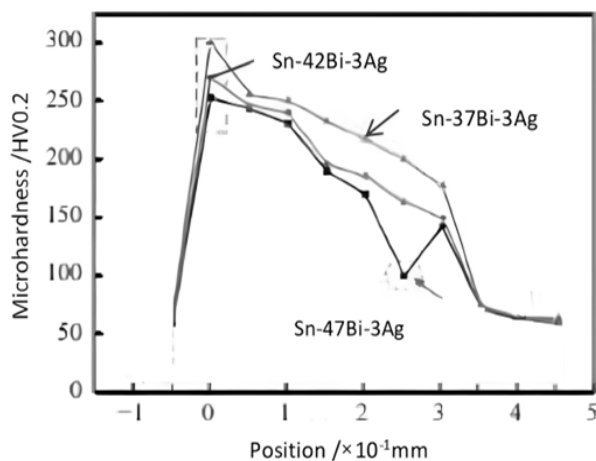


Fig. 6 Microhardness distribution curve

## 5 Conclusion

In this paper, the microstructures and mechanical properties of solar panel busbar laser soldering joints were analyzed by using different coated brass solders, and the mechanism of Bi element in unleaded tin-coated copper stitch soldering was revealed. The main conclusions are:

- When the continuous single-mode laser is selected, the power is 400W, the wavelength is 1080nm, and the soldering speed is 10mm/s, the morphology quality of unleaded tin-coated copper with brass solder Sn-47Al-3Ag is best, and the front side of the soldering joint is smooth and plump, the back side is continuous and has no obvious defects. The cross

section morphology of the joint has obvious characteristics of fusion soldering and brazing.

- The soldering joint of unleaded tin-coated copper can be divided into interconnection belt fusion weld zone, weld center zone and busbar brazing weld zone. There is an Ag<sub>3</sub>Sn phase intermetallic compound layer in the busbar brazing weld zone. With the increase of Bi element content, the massive area (Bi element) in the alloy structure is increasing, the segregation is more obvious, and the thickness of intermetallic compound layer is decreasing.
- The fracture of welded joints is at the interconnection belt side, and the maximum tensile strength of the joints is 212Mpa. With the decrease of Bi element content, the tensile strength gradually increases. The maximum microhardness of the weld zone appears at the interface layer, and the microhardness of the weld zone increases with the decrease of Bi element content.

Furthermore, this paper can continue to discuss the influence of solder composition Ag element, soldering power, soldering speed and other process parameters on the microstructure and mechanical properties of solar panel busbar laser soldering.

## References

- [1] BIRAM DIENG, JEAN PIERRE TINE, SENGHANE MBODJI. (2020). Solar panels optimization for a better efficiency and for hot water production: Determination of the exchange coefficient [J]. *International Journal of Engineering & Technology*, Vol. 12, No. 3, pp. 476-482.
- [2] SKUPOV A. A., PANTELEEV M. D., SHCHERBAKOV A. V. (2022). Laser soldering of fuselage panels from aluminum V-1579 and aluminum-lithium V-1481 alloys [J]. *Soldering International*, Vol. 36, No. 2, pp. 92-96.
- [3] JADHAV SURAJ DINKAR, FU DONGMEI, DEPREZ MAXIM. (2020). Highly conductive and strong CuSn0.3 alloy processed via laser powder bed fusion starting from a tin-coated copper powder [J]. *Additive Manufacturing*, Vol. 36, pp. 101607.
- [4] BAI YUTAN. Design and analysis of mechanical system for automatic soldering production

- line of solar panel busbar [D]. Ningxia: Ningxia University, 2020.
- [5] WANG LIHENG. Design of automatic soldering production line for solar panel bus-stripe and research on the bus-stripe soldering process [D]. Ningxia: Ningxia University, 2021.
- [6] WANG MENG. Design and simulation of feeding device for battery series in solar panel confluence belt soldering prouduction line [D]. Ningxia: Ningxia University, 2022.
- [7] IHOR MYS, MICHAEL SCHMIDT. (2006). Laser micro soldering of copper and aluminum [J]. *Laser-based Micropackaging*, Vol. 6107, pp. 28-33.
- [8] BALASUBRAMANIAN K.R., SUTHAKAR T., SANKARANARAYANASAMY K. (2011). Laser soldering Simulations of Stainless Steel Joints Using Finite Element Analysis [J]. *Advanced Materials Research*, Vol. 383, pp. 6225-6230.
- [9] ZHOU L, LUO L Y, TAN C W, et al. (2018). Effect of soldering speed on microstructural evolution and mechanical properties of laser welded-brazed Al/brass dissimilar joints [J]. *Optics and Laser Technology*, Vol. 98, pp. 234-246.
- [10] SCHMALEN P, PLAPPER P. (2016). Evolution of laser braze-welded dissimilar Al-Cu joint. [J]. *Physics Procedia*, Vol. 83, pp. 506-514.
- [11] ZHAO YANGXIAO. Research on the laser folding soldering process of the fuel cell stainless steel ultra-thin bipolar plate [D]. Hunan: Hunan Institute of Science and Technology, 2021.
- [12] HE LINJI, ZHANG TIANLEI, XU GANG. (2021). Numerical simulation of dynamic behavior of molten pool in laser deep penetration soldering [J]. *Intelligent Computer and Applications*, Vol. 11, No. 3, pp. 125-133.
- [13] WANG ZHENGtian, JIANG SHUYUAN, CHEN YIPING. (2021). Numerical simulation of laser soldering of magnesium and steel dissimilar metal based on ABAQUS [J]. *Journal of Material Heat Treatment*, Vol. 42, No. 7, pp. 135-142.
- [14] LI LINGSHAN. Numerical simulation of TC4 borders-hatch multiple-tracks scanning in SLM processing based on lattice Boltzmann method [D]. Beijing: Beijing University of Technology, 2020.
- [15] ANIL KUNWAR, AN LILI, LIU JIAHUI. (2020). A data-driven framework to predict the morphology of interfacial Cu<sub>6</sub>Sn<sub>5</sub> IMC in SAC/Cu system during laser soldering [J]. *Journal of Materials Science & Technology*, Vol. 50, No. 15, pp. 115-127.
- [16] T.J.NABILA, S.R.A.LDRIS, M.ISHAK. (2019). Effect of fibre-lasers Parameters on interfacial reaction and wetting angle of two different types of SAC305 solder fabrication on Cu Pad [J]. *IOP Conference Series: Materials Science and Engineering*, Vol. 469, No. 1, pp. 11674.
- [17] MARTIN J.B. (2017). Electrical resises of soldered battery cell connections [J]. *Journal of Energy Storage*, Vol. 12, pp. 45-54.
- [18] ZHOU YUHAO, WU MINGFANG, PU JUAN. (2023). Effect of Al Content in Zn-Al Flux-Cored soldering Wire on Microstructure and Properties of Al/Cu Laser soldering Brazed Joints[J]. *Hot Working Technology*, Vol. 52, No. 13, pp. 131-135.
- [19] PAVEL HOUSKA, et al. (2024). The Effect of Laser Welding Parameters on Aluminium PV Construction Rack Systems [J]. *Manufacturing Technology*, Vol.24, No. 1, pp. 47-52.
- [20] IKHSAN SIREGAR, JURI SAEDON, MOHD SHAHRIMAN ADENAN. (2025). Milling Performance of Selective Laser Melted Ti6Al4V: A Taguchi Approach for Surface Roughness Optimization [J]. *Manufacturing Technology*, Vol.25, No. 2, pp. 230-238.
- [21] ONDREJ BILEK, JAN ONDRIK, PETR JANIK, TOMAS KAUTSKY. (2024). Micro-texturing for Enhanced Machining: Evaluating Tool Performance in Laser-Processed Cutting Inserts [J]. *Manufacturing Technology*, Vol.24, No. 2, pp. 173-182.